Digital Object Identifier (DOI): 10.1109/TIE.2018.2816008

IEEE Transaction on Industrial Electronics (Volume: 65, Issue: 12, Dec. 2018)

Passivity-based Control of Switched Reluctance-based Wind System Supplying Constant Power Load

Mohammad Masoud Namazi
Sayed Morteza Saghaian Nejad
Ahmadreza Tabesh
Amir Rashidi
Marco Liserre

Suggested Citation

M. M. Namazi, S. M. S. Nejad, A. Tabesh, A. Rashidi and M. Liserre, "Passivity-Based Control of Switched Reluctance-Based Wind System Supplying Constant Power Load," in *IEEE Transactions on Industrial Electronics*, vol. 65, no. 12, pp. 9550-9560, Dec. 2018.

Passivity-based Control of Switched Reluctance-based Wind System Supplying Constant Power Load

Mohammad Masoud Namazi, *Student Member*, *IEEE*, Sayed Morteza Saghaian Nejad, Ahmadreza Tabesh, *Member*, *IEEE*, Amir Rashidi, and Marco Liserre, *Fellow*, *IEEE*

***Abstract*—This paper presents a passivity-based control (PBC) scheme for the Switched Reluctance Generator (SRG) in small-scale wind energy conversion systems (WECSs) for DC microgrid application. The main objective is to stabilize the output voltage in case the system supplies constant power loads (CPLs) and operates with maximum power point tracking (MPPT). Stability improvement and dc-link ripple reduction in the presence of CPLs is achieved using system level modeling of SRG-based DC microgrid through the Euler-Lagrange system (ELS) from the view point of the machine physical structure. Compared with other control methods, the proposed MPPT method based on passivity-based speed controller employs the back-EMF in the generation process as a position-dependent voltage source to overcome the major challenge of SRG complicated uncertain dynamic model. To deal with the time-varying inductance and back-emf of SRG, an adaptation mechanism is incorporated in proposed adaptive PBC and the control design is constructed by using the Lyapunov theorem where the closed-loop stability is ensured. The effectiveness of the proposed method in avoiding instability effects of SRG and CPL with voltage ripple reduction and precise wind turbine speed tracking is investigated with simulation results and validated with experimental by using a four-phase, 8/6 SRG drive system.**

Switched Reluctance Generator (SRG); Wind turbine; Passivity-based control; Constant-power load.

I. Introduction

Switched reluctance machines (SRM) are being increasingly considered as candidates for small-scale DC-based WECS due to their advantages such as no need for rare-earth permanent magnets, low cost, high reliability, and dc-like output voltage [1]. Moreover, they do not need a gearbox due to their high pole structure, which allows wind turbines to be installed also in environmental conditions which could be very challenging for the gearbox [2]. Since modern loads require a dc input, DC-based architectures provide a more natural option for integration of most new distributed generation sources and energy storage devices that provide an inherently dc output. However, the dynamic interaction effects of distributed generation sources and loads are the main source of instability in DC microgrids.

The self-excitation operation of SRG tends to become instable, when the dc-link energy is not sufficient to excite the SRG phases under heavy load conditions, or when the back-EMF is higher than the source voltage. The instability problem is aggravated by the integration of a variety of tightly-regulated power electronic converters as the constant power load and nonlinearity due to negative input resistance. A SRG-based DC microgrid with a dc-link ripple reduction is proposed in [3] in which Proportional-Integral (PI) control and an energy storage system is used. However, the interaction effect of the nonlinear dynamic characteristics of WECS and constant power loads on the stability of the output voltage has been ignored in this microgrid. The performance of SRG-based aircraft power systems in the presence of a constant power load was studied using a behavioral modeling in [4] but no solution was proposed for reducing the dc-link fluctuations. For the above-mentioned control strategy, the uncertain SRG parameters were linearized and the stability of the output voltage was ignored. Due to the unstable characteristics of CPLs, linear stabilization methods are not effective and nonlinear large-signal analysis are only being used.

In [5], a passive stabilization method is used using passive components such as RC and RL parallel dampers, which is plagued by reduced system efficiency. To avoid reduced efficiency, an active damping approach is proposed in [6] by injecting a compensating current using an auxiliary line regulating circuit (LRC), which makes the system complicated. In [7], an efficient method is proposed for reducing the CPL effect as an active damping by increasing the load resistance based on a supercapacitor energy storage system. The sliding mode control has also been applied as a different active damping approach for the control and large signal analysis to enhance the output voltage stability [8]. A variety of active damping methods have been proposed to eliminate excess energy in the dc-link during severe transients [9].

Many studies have been devoted to the evaluation of SRG-based WECS performance [10]. However, the time-varying uncertainties associated with the complicated dynamic model have not been duly considered. Unlike other common AC generators, the back-EMF of SRG in the generating process is a time-varying, position-dependent voltage source that results in

Manuscript received September 14, 2017; revised November 22, 2017 and February 1, 2018; accepted February 28, 2018. (Corresponding author: Mohammad Masoud Namazi)

M. M. Namazi, S. M. Saghaian Nejad, A. Tabesh and A. Rashidi are with the Department of Electrical and Computer Engineering, Isfahan University of Technology, Isfahan, 84156-83111, Iran (e-mail: mm.namazi@ec.iut.ac.ir, saghaian@cc.iut.ac.ir, a.tabesh@cc.iut.ac.ir, a.rashidi@ec.iut.ac.ir).

M. Liserre is with the Chair of Power Electronics, Christian-Albrechts University of Kiel, Kiel, Germany (e-mail: ml@tf.uni-kiel.de).

a complicated model that cannot be ignored in MPPT strategy as has been the case in large-scale WECSs. Although small-signal analysis methods provide an effective way to investigate the stability at the equilibrium point, they cannot be employed in the presence of time-varying back-EMF dynamics. The passivity-based control has been instead proposed as a useful large-signal stability analysis method with robustness against parameters uncertainties. Moreover, passivity-based control using Port-controlled Hamiltonian System (PCHS) and Euler-Lagrange modeling has been proposed to provide a generalized integrated structure focus on source dynamic [11], and on load dynamic [12]. A classic passivity-based control is designed [13] for small-scale WECS systems considering the generator dynamics. However, the MPPT and dc-link voltage control has been designed without taking into account the CPL effect.

In this paper, a new approach is proposed for the control of self-excited SRG in a small-scale WECS. To achieve voltage stability enhancement and voltage ripple reduction as well as the MPPT operation, the PBC is designed through Euler-Lagrange system realization. Conventional MPPT control methods are based on a linearized model of the system about an operating point and ignore the back-emf nonlinear terms by treating them as disturbance ones. The proposed PBC-based MPPT method is inherently nonlinear and covers a wide range of operating points while both back-emf nonlinear terms and the controller design procedure are considered in the model. The system-level EL modeling of SRG-based DC microgrid is fulfilled with regard to the interaction of SRG and nonlinear CPL. Also, in order to take into account the SRG uncertainty in the position-dependent time-varying back-emf, an adaptation mechanism is added to the PBC method. Finally, the validity and effectiveness of the proposed control approach are demonstrated through simulation and experimental results.

II. Dynamic Model of DC Microgrid Switched Reluctance Generator-Based WECS

The overall layout of the proposed SRG-based WECS structure is shown in Fig. 1. The DC microgrid circuit includes an energy storage, a bulk dc-link capacitor, and a constant power load which is directly connected to this link. It is assumed that the SRG operates in the self-excited mode and is connected to the dc-link considered as a dc-dc integrated boost converter. The storage unit, including the lead-acid batteries, is connected to the dc-link through a dc-dc bidirectional converter. Lead-acid batteries presently form the dominant, economically viable energy storage technology offering such advantages as low price, stable performance, and operation under a wide range of temperatures. The use of a bidirectional converter in the proposed system is based on the following reasons: 1) the dc-link voltage is not necessarily equal to that of the battery under all conditions; and 2) in the case of supplying CPL, the dc-link voltage fluctuations are severe and the charge and discharge of the battery experience higher ripples. The use of the converter will, therefore, help mitigate these fluctuations via a feedback control loop.

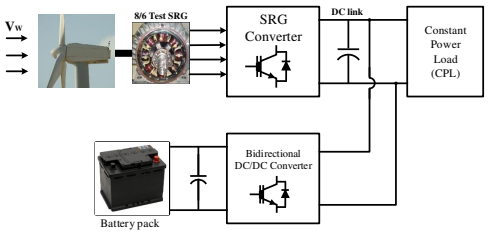

Fig. 1. Basic model of the wind-driven SRG-based DC microgrid.

A. Dynamic Model of Wind-driven SRG

The basic sets of electrical and mechanical differential equations are used for dynamic modeling of SRG. The mechanical torque, T_m, applied to the wind turbine shaft is as follows

$$T_m = \frac{1}{2}\rho AR\frac{C_p(\lambda)}{\lambda}V_w^2 \tag{1}$$

where, ρ is air density, A is the area swept by the blades, $C_p(\lambda)$ is the power coefficient, $\lambda = \frac{R\omega_m}{V_w}$ is the tip speed ratio, and V_ω is the wind speed. R and ω_m denote turbine blade radius and shaft's rotational speed, respectively. The generator state-space dynamic model can be expressed by

$$J\dot{\omega}_m = T_m - \sum_{j=1}^{4} T_{ej}(\theta, i_j), \tag{2}$$

$$L_j(\theta)\frac{di_j}{dt} = u_j - ri_j - \frac{dL_j(\theta)}{d\theta}i_j\omega_m. \tag{3}$$

where, u is the phase voltage, i denotes the phase current, r stands for the phase resistance, J is the inertia, and $j = 1, 2, 3, 4$ stands for each phase of the machine. The phase inductance function, $L_j(\theta)$, is usually obtained by a lookup table. Assuming that the machine operates at relatively low current levels, it is functionally approximated using below

$$L_j(\theta) = l_0 - l_1 cos(N_r\theta - (j-1)\frac{2\pi}{3}) \tag{4}$$

where, θ denotes the rotor position, $l_0 > l_1$ are positive values, N_r is the number of rotor poles, and $k_j(\theta)$ is defined as

$$k_j(\theta) = \frac{\partial L_j}{\partial\theta} = N_r l_1 sin(N_r\theta - (j-1)\frac{2\pi}{3}) \tag{5}$$

Finally, the SRG phase torque T_e is expressed by

$$T_{ej}(\theta, i_j) = \frac{1}{2}i_j^2\frac{dL_j(\theta)}{d\theta} = \frac{1}{2}i_j^2 k_j(\theta) \tag{6}$$

B. Aggregated Dynamic Model

At a constant power load when the input voltage increases, the current decreases, and vice versa. Thus, this equipment has a negative incremental resistance, which can lead to declining damping and instability. The asymmetric converter in the self-excited operation mode can be considered as a DC-DC integrated boost converter as shown in Fig. 2(a). The

DC microgrid structure with the equivalent one-phase self-excited boost operation of SRG is shown Fig. 2(b). The overall dynamic state equations of the system can be represented by

$$L_j(\theta)\frac{di_j}{dt} = -ri_j - (1-d_j)V_c + \omega_m i_j k_j(\theta), \quad (7)$$

$$L_b\frac{di_b}{dt} = V_b - (1-d_b)V_c - i_b R_b, \quad (8)$$

$$C_{dc}\frac{dV_c}{dt} = \sum_{j=1}^{4}(1-d_j)i_j + (1-d_b)i_b - i_{cpl}, \quad (9)$$

$$J\dot{\omega}_m = \frac{1}{2}\rho AR\frac{C_p(\lambda)}{\lambda}V_w^2 - \frac{1}{2}\sum_{j=1}^{4} i_j^2 k_j(\theta). \quad (10)$$

where, d_j and d_b denote the switching signal as the control input to the SRG converter and the bidirectional converter respectively, V_c is the dc-link voltage, C_{dc} is the dc-link capacitor, i_b is the battery current, R_b is the battery internal resistance, L_b is the bidirectional converter inductance, and $i_{cpl} = P_{cpl}/V_c$ is the current of the constant power load. The time constant of the batteries used is about 800 ms but the system dynamics is in the order of 100 ms. Thus, the battery can be envisioned as a constant voltage source, V_b, within the frequency range of the system dynamics.

The self-excitation operation of SRG has a tendency toward instability in heavy loads when the dc-link energy is not sufficient to excite he SRG phases. The Frequency response of SRG small-signal model in light (260 W) and heavy (1200 W) loads are shown in Fig. 3(a) and (b). As elaborated in [4], the transfer function of SRG can be obtained based on system identification techniques. However, since there is no need for the analytical form of the transfer function, the numerical method based on MATLAB/SIMULINK linear analysis toolbox [14] is preferred for obtaining the frequency response. The SRG current and the dc-link voltage are considered as input and output variables, respectively. The cause underlying the instability observed is the CPL, which exhibits a negative resistive behavior. The adverse effect of this negative resistance becomes significant especially at heavy CPLs. It is clear from Fig. 3 that the phase margin starts from $34.8°$ for a light load down to zero for a heavy load. Moreover, as shown in Fig. 3 (b), the phase diagram starts from a phase lower than $-180°$, which is shown two poles at the origin and the system is, therefore, unstable.

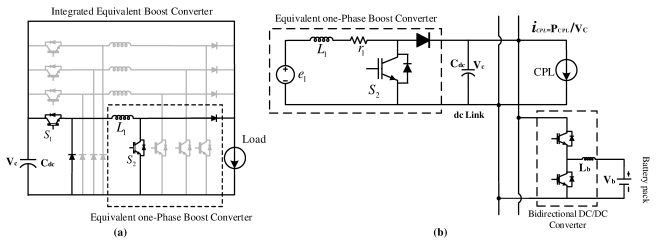

Fig. 2. The integrated structure of a self-excited SRG asymmetric converter, (a) complete four phase, (b) the equivalent one-phase boost operation of the SRG-based DC microgrid.

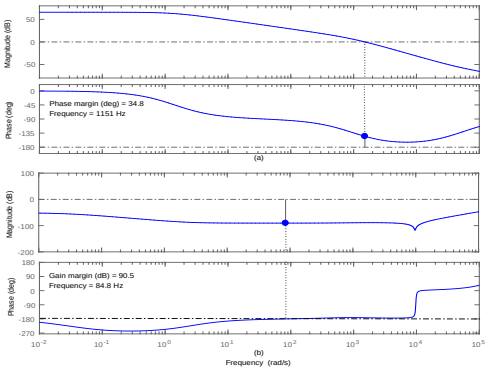

Fig. 3. Frequency response of the self-exited SRG; (a) Stable in light CPL (260 W), (b) Unstable in heavy CPL (1200 W).

III. Proposed Passivity-Based Controller Design of Studied DC Microgrid SRG-based WECS

The SRG-based DC microgrid is inherently a nonlinear system with coupled dynamic model which the operating point is widely changed in WECS applications. The PBC is introduced to achieve stability by energy shaping and damping injection through a energy function as a lyapunov-like function minimized at the desired equilibrium points. In order to design the dc-link voltage and the speed control of the SRG, the EL representations of (7) to (10) are derived as an integrated mathematical model to describe the dynamics of the aggregated wind-driven SRG and bidirectional dc-dc converter which is supplying CPL. However, the limitation of the proposed PBC is that it is not appropriate when the location of storage unit is far from the wind turbine. The speed of the SRG is controlled to achieve MPPT only through generator controller, while the dc-link voltage is controlled using both generator and dc-dc converter controllers considering SRG and CPL dynamics, simultaneously. In fact, the controller of the dc-link is designed based on the proposed integrated PBC considering the effects of SRG, energy storage, and constant power load.

A. ELS model

By defining a control vector when $u_j = 1-d_j$ is considered as the duty cycle of S_2 and $u_b = 1-d_b$ as that of the bidirectional converter, and when $x = [i_j, i_b, V_c, \omega_m]^T$, the system in (7-10) can be described in the form of an ELS [15]

$$D\dot{x} + J(u,x)x + R(x)x = G \quad (11)$$

where,

$$D = \begin{bmatrix} L_j(\theta) & 0 & 0 & 0 \\ 0 & L_b & 0 & 0 \\ 0 & 0 & C_{dc} & 0 \\ 0 & 0 & 0 & 2J \end{bmatrix}, \quad G = \begin{bmatrix} 0 \\ V_b \\ 0 \\ 2T_m \end{bmatrix}.$$

The dissipation effects are captured by the matrix $R^T(x) = R(x)$, where,

$$R(x) = \begin{bmatrix} r & 0 & 0 & 0 \\ 0 & R_b & 0 & 0 \\ 0 & 0 & \frac{P_{cpl}}{V_c^2} & 0 \\ 0 & 0 & 0 & 0 \end{bmatrix}.$$

Moreover, the interconnection structure is captured by the matrix $J(u,x)$ as

$$J(u,x)=\begin{bmatrix} 0 & 0 & u_j & -i_j k_j(\theta) \\ 0 & 0 & u_b & 0 \\ -u_j & -u_b & 0 & 0 \\ i_j k_j(\theta) & 0 & 0 & 0 \end{bmatrix}=$$

$$\overbrace{\begin{bmatrix} 0 & 0 & 0 & -i_j k_j(\theta) \\ 0 & 0 & 0 & 0 \\ 0 & 0 & 0 & 0 \\ i_j k_j(\theta) & 0 & 0 & 0 \end{bmatrix}}^{J_0(x)}+$$

$$\overbrace{\begin{bmatrix} 0 & 0 & 1 & 0 \\ 0 & 0 & 0 & 0 \\ -1 & 0 & 0 & 0 \\ 0 & 0 & 0 & 0 \end{bmatrix}}^{J_1} u_j+\overbrace{\begin{bmatrix} 0 & 0 & 0 & 0 \\ 0 & 0 & 1 & 0 \\ 0 & -1 & 0 & 0 \\ 0 & 0 & 0 & 0 \end{bmatrix}}^{J_2} u_b,$$

In which the skew-symmetric condition is held as $J_i=-{J_i}^T, \quad i=0,1,2.$

B. DC-link Voltage Control Supplying Constant Power Load

The dc-link voltage controller is designed considering all relevant dynamics of SRG, and energy storage. The presence of CPL further increases the nonlinearity of the bidirectional converter system, which in turn increases the challenge for the control. In such a situation, controllers designed through linear approaches are insufficient, and the controller of the SRG and bidirectional converter should have sufficient stability margins to ensure the stability in a large-signal sense. Therefore, the main advantage of the proposed PBC is to consider all of the system dynamics in an unified control design algorithm to dc-link voltage ripples reduction and improving its stabilization. The first step is to modify the Hamiltonian function assigned to the closed-loop system by the following energy function

$$H(x)=\frac{1}{2}\tilde{x}^T D\tilde{x}$$

Taking the derivative yields

$$\begin{aligned}\dot{H}(x)&=\tilde{x}^T D\dot{\tilde{x}}+\tfrac{1}{2}\tilde{x}^T\dot{D}\tilde{x}\\ &=-\tilde{x}^T[J_0(x)+J_1u_1+J_2u_2+R(x)+R_i(x)]\tilde{x}\\ &+\tfrac{1}{2}\tilde{x}^T\begin{bmatrix}\omega_m k_j(\theta) & 0 & 0 & 0\\ 0 & 0 & 0 & 0\\ 0 & 0 & 0 & 0\\ 0 & 0 & 0 & 0\end{bmatrix}\tilde{x}\end{aligned}$$

With the property $\tilde{x}^T J(u,x)\tilde{x}=0$ and selecting $R_i(x)$ as $R_d=R(x)+R_i(x)$, and due to the negative slope of the SRG inductance profile which yields $k_j(\theta)<0$, we have $\dot{H}(x)\leq -\tilde{x}^T R_d\tilde{x}-\eta\leq -\lambda-\eta<0$, where λ and η are positive constants. This means that the system is strictly passive and that the error exponentially tends to zero as a result of the PBC, which demonstrate the intrinsical stability of passive type system. The states of the nonlinear dynamic model developed in (11) can be decomposed into a controlled state x_c and the free states x_f as $x=[x_c \quad x_f]$. With such a subdivision, the equation describing the control (11) may also be divided up as follows [16]

$$\begin{aligned}&D_c\dot{x}_c+\left[J_{c0}(x)+J_{c1}u_1+J_{c2}u_2\right]x_c+\\ &R_c(x)x_c+J_{cf}u_b x_f=G_c,\\ &D_f\dot{x}_f+\left[J_{f0}(x)+J_{f1}u_1+J_{f2}u_2\right]x_f+\\ &R_f(x)x_f+J_{fc}u_b x_f=G_f,\end{aligned}\tag{12}$$

Let x^d denote the desired equilibrium. The error vector can then be calculated with respect to this equilibrium as $\tilde{x}=x-x^d$. Assuming the x_c^d and x_f^d to be the desired values for the controlled and free states, respectively, (12) can be rewritten for the first subsystem as

$$\begin{aligned}&G_{c1}+R_{ic1}\tilde{x}_{c1}-(D_{c1}\dot{x}_{c1}^d+\\ &[J_{c10}(x)+J_{c11}u_j+J_{c12}u_b+R_{c1}(x)]\,x_{c1}^d+J_{cf1}u_b x_f^d)=0,\\ &G_{f1}+R_{if1}\tilde{x}_{f1}-(D_{f1}\dot{x}_{f1}^d+\\ &[J_{f10}(x)+J_{f11}u_j+J_{f12}u_j+R_{f1}(x)]\,x_{f1}^d+J_{fc1}u_b x_c^d)=0,\end{aligned}\tag{13}$$

For the regulation problem, it is observed that $\dot{x}_{c1}^d=0$. One can compute the control signal u_b as

$$u_b=f(x_{c1}^d,x_{f1}^d,G,R_{ic1}\tilde{x}_{c1})\tag{14}$$

where, the free mode dynamics, x_f^d, is expressed by

$$\begin{aligned}&\dot{x}_f^d=-D_{f1}^{-1}(J_{fc1}u_b x_{c1}^d-R_{if1}(x)\tilde{x}_{f1})\\ &+D_{f1}^{-1}.(G_{f1}-[J_{f10}(x)+(J_{f11}+J_{f12})u_j+R_{f1}(x)]\,x_{f1}^d)\end{aligned}\tag{15}$$

For the system to be globally stable, zeros dynamics must converge, which means that application of $u_b\mapsto x_f^d$ is passive. The states of the first subsystem including the generator and the battery storage systems can be represented by $x_{c1}=i_b$ and $x_{f1}=V_c$ whose desired values are denoted by $x_{c1}^d=i_b^*$ and $x_{f1}^d=V_c^d$. In fact, the internal generated dc-link voltage dynamic is denoted by superscript (d) against the externally fixed reference battery current which is denoted by superscript $(*)$ [17]. Consider (13) with the following parameters

$$\begin{aligned}&D_{c1}=L_j\,(\theta)\,, G_{c1}=V_b, R_{c1}=R_b, R_{ic1}=R_{i2}\\ &J_{c10}=J_{c11}=0, J_{c12}=J_{cf1}=J_{cf1}=1\\ &D_{f1}=C_{dc},\, G_{f1}=0, J_{f10}=J_{f11}=J_{f12}=0, J_{fc1}=1,\\ &R_{f1}(x)=\tfrac{P_{cpl}}{V_c^2}, R_{if1}=\tfrac{1}{R_{i3}}-\tfrac{P_{cpl}}{V_c^2}\end{aligned}$$

This constructs the desired system expressed by

$$\begin{aligned}&V_b-R_b i_b^*-u_b V_c^d+R_{i2}(i_b-i_b^*)=0,\\ &-C_{dc}\dot{V}_c^d+u_b i_b^*=\tfrac{P_{cpl}}{V_c}-\tfrac{1}{R_{i3}}(V_c-V_c^d).\end{aligned}\tag{16}$$

From (16), the control input $u_c=d_b$ can be calculated as

$$d_b=1-\frac{1}{V_c^d}\left(V_b-R_b i_b^*+R_{i2}(i_b-i_b^*)\right)\tag{17}$$

The dynamics of the desired free variables used in the control law is obtained from (16) and (17) as follows

$$\dot{V}_c^d=\tfrac{1}{C_{dc}}(u_b i_b^*+\tfrac{1}{R_{i3}}(V_c-V_c^d)-\tfrac{P_{cpl}}{V_c})\tag{18}$$

To ensure internal stability, it is necessary to prove that the zero dynamic's of the system's output (i.e., that state of the

system that has been fixed) is asymptotically stable [18]. The conditions for the internal stability of (17) should be taken into account when the dc-link voltage is the output. The system is then asymptotically stable at the equilibrium point i_b^*. When the error is zero, (18) can be rewritten as

$$\dot{V}_c^d = \frac{1}{C_{dc}}(u_b i_b^* - \frac{P_{cpl}}{V_c^d})$$

Substituting of u_b from (17) in the above relation, yields

$$\dot{V}_c^d = \frac{1}{C_{dc}V_c^d}\left(i_b^*\left(V_b - R_b i_b^*\right) - P_{cpl}\right)$$

The relation derived from the requirement that the stable equilibrium point is achieved will be as $P_{cpl} < i_b^*\left(V_b - R_b i_b^*\right)$.

C. MPPT Realization

The initial step in the passivity-based control design involves the tracking of the generator's voltage toward its desired value. However, the wind-driven SRG controller is designed to achieve the MPPT, this controller beside the energy storage controller are used for controlling the dc-link voltage, simultaneously. In this process, based on the guaranteed stability of dc-link voltage, the PBC is designed to control the rotor speed of wind generator at its optimum value of $\omega_m^d = \lambda_{opt} V_w$ in order to realize MPPT operation. The corresponding reference phase current is obtained from the torque to current look-up table or by the invertible SRM model. This subdivides of the system states into two subsystems with $x_{c2} = i_j$ and $x_{f2} = [V_c \quad \omega_m]^T$. Hence, using (13), the reference (desired) values for the interconnected system are $x_{c2}^d = i_j^*$ and $x_{f2}^d = [V_c^d \quad \omega_m^d]^T$. A difference is noted between i_j^*, which is constant in the case of a regulation task where $\dot{x}_{c2}^d = \dot{i}_j^* = 0$, and the desired output values, $[V_c^d \quad \omega_m^d]^T$, which exhibits the system dynamics depending on the control input. Relation (13) can be used for the second subsystem as follows

$$\begin{array}{l} G_{c2} + R_{ic2}\tilde{x}_{c2} - \\ \left(D_{c2}\dot{x}_{c2}^d + \left[J_{c20}(x) + J_{c21}u_j + J_{c22}u_b + R_{c2}(x)\right]x_{c2}^d + \right. \\ \left. + \left(J_{cf20}(x) + J_{cf21}[u_j \quad 0]x_f^d\right) = 0, \right. \\ G_{f2} + R_{if2}\tilde{x}_{f2} - \\ \left(D_{f2}\dot{x}_{f2}^d + \left[J_{f20}(x) + J_{f21}u_j + J_{f22}u_j + R_{f2}(x)\right]x_{f2}^d + \right. \\ \left. + J_{fc20}(x) + J_{fc21}\begin{bmatrix} u_j \\ 0 \end{bmatrix} x_c^d\right) = 0, \end{array}$$

The second dynamical Euler-Lagrange subsystem including dc-link, CPL, and SRG can be represented by

$$\begin{array}{l} ri_j^* + \left(\begin{bmatrix} 0 & -k_j(\theta)\, i_j \end{bmatrix} + \begin{bmatrix} u_j & 0 \end{bmatrix}\right)\begin{bmatrix} V_c^d \\ \omega_m^d \end{bmatrix} \\ -R_{ic2}(i_j - i_j^*) = 0, \end{array}$$

$$\begin{array}{l} \begin{bmatrix} C_{dc} & 0 \\ 0 & 2J \end{bmatrix}\begin{bmatrix} \dot{V}_c^d \\ \dot{\omega}_m^d \end{bmatrix} + \left(\begin{bmatrix} 0 \\ -k_j(\theta)\, i_j \end{bmatrix} + \begin{bmatrix} -u_j \\ 0 \end{bmatrix}\right) i_j^* \\ + \frac{1}{V_c^2}\begin{bmatrix} P_{cpl} & 0 \\ 0 & 0 \end{bmatrix}\begin{bmatrix} V_c^d \\ \omega_m^d \end{bmatrix} \\ = \begin{bmatrix} 0 \\ 2T_m \end{bmatrix} + \begin{bmatrix} \frac{1}{R_{i3}} - \frac{P_{cpl}}{V_c^2} & 0 \\ 0 & R_{i4} \end{bmatrix}\begin{bmatrix} V_c - V_c^d \\ \omega_m - \omega_m^d \end{bmatrix}. \end{array} \tag{19}$$

where,

$$\begin{array}{l} G_{c2} = 0, J_{c20} = J_{c21} = J_{c22} = \begin{bmatrix} 0 & 0 \end{bmatrix}, R_{c2} = r, \\ J_{cf20}(x) = \begin{bmatrix} 0 & -k_j(\theta)\, i_j \end{bmatrix}, J_{cf21} = 1, R_{ic2} = R_{i1} \\ D_{f2} = \begin{bmatrix} C_{dc} & 0 \\ 0 & 2J \end{bmatrix}, G_{f2} = \begin{bmatrix} 0 \\ 2T_m \end{bmatrix}, \\ J_{f20} = J_{f21} = J_{f22} = 0, J_{fc20}(x) = \begin{bmatrix} 0 \\ -k_j(\theta)\, i_j \end{bmatrix}, \\ J_{fc21} = 1, R_{f2}(x) = \frac{1}{V_c^2}\begin{bmatrix} P_{cpl} & 0 \\ 0 & 0 \end{bmatrix}, \\ R_{if2}(x) = \begin{bmatrix} \frac{1}{R_{i3}} - \frac{P_{cpl}}{V_c^2} & 0 \\ 0 & R_{i4} \end{bmatrix} \end{array}$$

From (19), the scalar differential equations of the second subsystem can be expressed as

$$\begin{array}{l} -ri_j^* - u_j V_c^d + k_j(\theta) i_j \omega_m^d + R_{i1}(i_j - i_j^*) = 0, \\ C_{dc}\dot{V}_c^d - u_j i_j^* - \frac{P_{cpl}}{V_c} + \frac{1}{R_{i3}}(V_c - V_c^d) = 0, \\ 2J\dot{\omega}_m^d - k_j(\theta) i_j i_j^* - 2T_m - R_{i4}(\omega_m - \omega_m^d) = 0. \end{array} \tag{20}$$

From (20), one can calculate the control input $u_j = 1 - d_j$

$$d_j = 1 - \frac{1}{V_c^d}\left(-ri_j^* + k_j(\theta) i_j \omega_m^d + R_{i1}(i_j - i_j^*)\right) \tag{21}$$

The dynamics of the desired free variables used in the control law are obtained from (20) and (21) as

$$\begin{array}{l} \dot{V}_c^d = \frac{1}{C_{dc}}\left(u_j i_j^* + \frac{1}{R_{i3}}(V_c - V_c^d) - \frac{P_{cpl}}{V_c}\right), \\ \dot{\omega}^d = \frac{1}{2J}\left(2T_m + k_j(\theta) i_j i_j^* + R_{i4}(\omega_m - \omega_m^d)\right) \end{array} \tag{22}$$

In order to prove the stability of the internal dynamics, it should be shown that the dc-link voltage and speed, as the outputs, are asymptotically stable at the equilibrium points i_j^*. Assuming $V_c = V_c^*$ and $\omega_m = \omega_m^*$, (9) can be expressed

$$0 = u_j {i_j}^* - \frac{P_{cpl}}{{V_c}^*} \rightarrow u_j = \frac{P_{cpl}}{{i_j}^* {V_c}^*}$$

By substituting the value thus obtained in (7), one obtain the following relation

$$-r{i_j}^* - \frac{P_{cpl}}{{i_j}^*} + {\omega_m}^* {i_j}^* k_j(\theta) = 0$$

The relation obtained based on the requirement that a stable equilibrium point is achieved will be as follows

$$\begin{array}{rl} P_{cpl} & < {\omega_m}^*\, {i_j}^*\, k_j(\theta) {i_j}^* - r\, {i_j}^{*2} \\ & = e\,(\theta)\, {i_j}^* - r\, {i_j}^{*2} \\ & = P_g - P_{loss} \end{array}$$

Based on the inequalities thus obtained, it may be concluded that the quantity of CPL should be less than net output power of the generator and the battery pack in order to ensure internal stability [19].

The damping injection formed by R_i is used to mitigate the dc-link voltage fluctuations and undershoots while also improving the stability margin of the system. Higher values of damping parameters provide smaller voltage ripples, dips, or overshoots. On the other hand, there is a trade-off between the smoothness and the speed of the tracking error convergence. The damping injection factor, R_i, should be selected between maximum and minimum damping bounds. The upper and lower bounds used in the implementation of PBCs are calculated by algebraic analysis [16], [18].

IV. Proposed Adaptive PBC for The Estimation of Uncertain SRG Parameters

As already mentioned Section II above, the $L_j(\theta)$ and $k_j(\theta)$ can be approximately calculated by (4) and (5), which is suitable for the low currents prior to the saturation region. In this section, an adaptive technique is presented to estimate these unknown parameters of SRG based on the proposed PBC method to overcome this type of parametric uncertainty. Unlike conventional methods, an adaptation mechanism is added to PBC which yields the novel adaptive classic PBC method as an alternative to other usual adaptive PBC methods [20]. In fact, in the proposed adaptive passivity-based control method, the controller design and adaptive mechanisms are aggregated. This is possible when the system is linear with respect to the estimated parameters. In this case, the Lyapunov stability is ensured as described below. By defining the vector P as the real parametric vector to be estimated, $\hat{P}$ becomes the related estimated value. The error of parameters is defined as $\tilde{P} = P - \hat{P}$, with the property $\dot{\tilde{P}} = -\dot{\hat{P}}$. The difference between two ELs, the subsystem that includes both the real and the estimated parameters can be expressed by

$$\Delta G - (\Delta D\dot{x}^d + \Delta J(x, u_c)x^d + \Delta R(x)x^d) \tag{23}$$

where, $\Delta(\cdot) = (\cdot) - (\hat{\cdot})$ denotes the error and if it converges to zero, stability is ensured. It is assumed that the system is linear in relation to the estimated parameters. Rearranging the right side of (23) by rewriting the parameter estimation error $\tilde{P}$ as

$$\Delta G - (\Delta D\dot{x}^d + \Delta Jx^d + \Delta Rx^d) = Y(\dot{x}^d, x^d, u_c)\tilde{P} \tag{24}$$

A candid Lyapunov function is defined as

$$V(\tilde{x}, \tilde{P}) = \frac{1}{2}\tilde{x}^T D\tilde{x} + \frac{1}{2}\tilde{P}^T\Gamma\tilde{P} \tag{25}$$

where, Γ is a positive semi-definite diagonal matrix. Using the properties of the passive system defined, the Lyapunov function derivative is obtained as

$$\dot{V}(\tilde{x}, \tilde{P}) = -\tilde{x}^T R_d\tilde{x} - \eta + \tilde{x}^T Y(\dot{x}^d, x^d, u_c)\tilde{P} - \tilde{P}^T\Gamma\dot{\hat{P}} \tag{26}$$

Hence, for $V(\tilde{x}, \tilde{P})$ to be a Lyapunov function, Relation (27) below must hold

$$\tilde{x}^T Y(\dot{x}^d, x^d, u_c)\tilde{P} - \tilde{P}^T\Gamma\dot{\hat{P}} = 0 \tag{27}$$

In this case, the control error converges to zero and the estimation error is stabilized around an equilibrium value. Condition (27) implicitly defines the parameter estimation law

$$\dot{\hat{P}} = \Gamma^{-1}Y^T(\dot{x}^d, x^d, u_c)\tilde{x} \tag{28}$$

The values of the diagonal positive semi-definite matrix Γ^{-1} define the estimated convergence speed. The adaptive passivity-based control thus developed is used to enhance the PBC designed here by estimating the time-varying parameters. Considering that $L_j(\theta)$ and $k_j(\theta)$ are the actual values of parameters to be estimated, the error parameters as $\tilde{L}_j(\theta) = L_j(\theta) - \hat{L}_j(\theta)$ and $\tilde{k}_j(\theta) = k_j(\theta) - \hat{k}_j(\theta)$ could be defined, in which $\hat{L}_j(\theta)$ and $\hat{k}_j(\theta)$ are the estimated values. Therefore, the error matrixes involved in the Euler-lagrange representation of (11) can be expressed as

$$\Delta H = \begin{bmatrix} \tilde{L}_j(\theta) & 0 & 0 & 0 \\ 0 & 0 & 0 & 0 \\ 0 & 0 & 0 & 0 \\ 0 & 0 & 0 & 0 \end{bmatrix}, \quad \Delta R = 0, \quad \Delta G = 0,$$

$$\Delta J = \begin{bmatrix} 0 & 0 & 0 & -i_j\tilde{k}_j(\theta) \\ 0 & 0 & 0 & 0 \\ 0 & 0 & 0 & 0 \\ -i_j\tilde{k}_j(\theta) & 0 & 0 & 0 \end{bmatrix}.$$

The first step is to use relation (24) with the defined error matrixes as in (29)

$$\begin{aligned} &\tilde{L}_j(\theta)\dot{x}_1^d + i_j\tilde{k}_j(\theta)x_4^d = Y_1, \\ &-i_j\tilde{k}_j(\theta)x_1^d = Y_2 \end{aligned} \tag{29}$$

which may be rendered in the matrix form below

$$Y(\dot{x}_{d1}, x_4^d) = \begin{bmatrix} \dot{x}_1^d & x_4^d \\ -x_1^d & 0 \end{bmatrix}, P = \begin{bmatrix} L_j(\theta) \\ k_j(\theta) \end{bmatrix}$$

Using (28), the parameter estimation law is calculated as

$$\frac{d}{dt}\begin{bmatrix} \hat{L}_j(\theta) \\ \hat{k}_j(\theta) \end{bmatrix} = \begin{bmatrix} g_1 & 0 \\ 0 & g_2 \end{bmatrix}\begin{bmatrix} \dot{x}_1^d & -x_1^d \\ x_4^d & 0 \end{bmatrix}\begin{bmatrix} i_j - i_j^* \\ \omega_m - \omega_m^d \end{bmatrix} \tag{30}$$

The positive constant parameters of matrix Γ^{-1}, i.e., g_1 and g_2, are selected based on the desired rate of estimation. To avoid oscillations, it is advantageous to use the minimum values that provide an acceptable estimation. Due to the existence of derivatives in the dynamics of $L_j(\theta)$, the term g_2 should be selected small enough to avoid oscillations.

V. Performance Evaluation

A. Description of the Study System

In order to evaluate the proposed PBC scheme, a SRG-based DC microgrid WECS system with the detailed parameters summarized in Table I is studied both by simulation and experimentally. The overall passivity-based control for the dc-link voltage and speed control based upon back-emf parameter estimation is shown in Fig. 4. Figure 5 shows the experimental setup that is provided to verify the performance of the proposed PBC. The battery pack consisting of four series of 12 V, 50 Ah Lead-Acid batteries with $R_b = 0.015\ \Omega$ is connected to a dc-link capacitor $C_{dc} = 400\ \mu F$ through the bidirectional dc-dc converter with $L_b = 0.63\ mH$ and switching frequency of 10 kHz. The wind turbine Properties are ρ = 1.225 kg/m^3, $\lambda_{opt} = 8.1$ and, $C_{p_{max}} = 0.35$. As can be seen in Table I, the mechanical damping coefficient of SRG equals the very low of 0.00013 Nms which may be neglected in the controller design. The validity of this assumption is verified by simulation and experimental results. The experimental SRG drive hardware is based on a floating-point TMS320F28335 DSP and consists of the following sections: (i) an asymmetrical converter is implemented by using IXYS 35N120A IGBT with a gate driver TLP250 and fast power diodes IXYS DSEI20-12 A; (ii) Hall-type galvanic

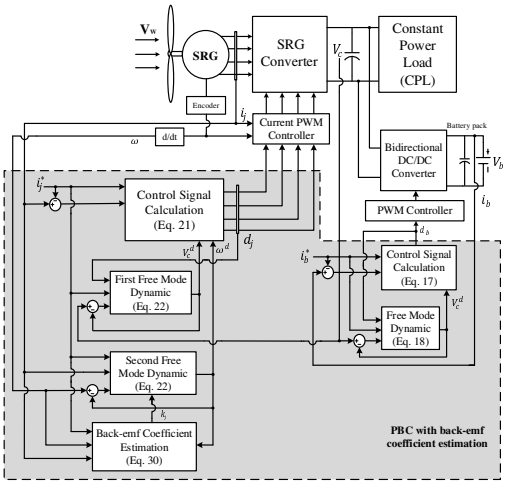

Fig. 4. Proposed PBC with back-emf coefficient estimation.

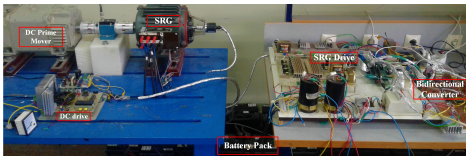

Fig. 5. Experimental test setup.

isolation CSNE151-104 Honeywell sensors for measuring the phase currents; and (iii) a 10-bit absolute encoder Autonics EP50S8 used to determine the rotor position. To emulate a wind turbine, a coupled 3.7 kW DC machine (DCM) is controlled through a ATmega16 AVR microcontroller-based drive with the full-bridge converter.

TABLE I
PARAMETERS OF SRG

Parameter	value
Rated Power	2.3 (kW)
Nominal DC Voltage	250 (V)
Nominal Current for cable sizing	9 (A rms)
Rated Speed	1500 (rpm)
Number of Stator/Rotor Poles	$8/6$
Phase Resistance	0.75 (Ω)
Mechanical Damping Factor (B)	0.00013 (Nms)

B. Results and Discussion

1) Simulation Results:

In the following, the MPPT strategy based on a real wind speed tracking with varying load power is studied. The control objectives are dc-link voltage regulation to 200 V and MPPT realization based on speed control of generator under a variable wind speed. The desired reference point for battery current, i_b^*, is obtained based on the power balance between the captured power by wind generator, power consumption by CPL, and the losses. The details for the calculation of i_b^* is given in Appendix.

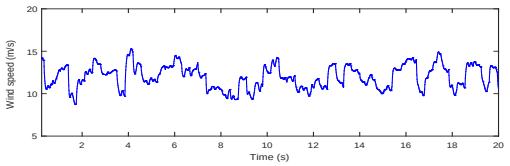

Fig. 6. The turbulent wind speed.

The turn-on angle is assumed to be constant and equal to 3°. Moreover, the first and second turn-off angles are 8° and 23°, respectively. In fact, as the main objective is not to maximize the generated power by the SRG, the switching angle is assumed to be constant. To achieve a maximum generated power with a minimum current ripple, a switching angle control algorithm should be used [21]. In this paper, the duty cycle d is the only parameter used in the PWM control approach to mitigate the CPL instability effect, similar to the approaches used in [22]. This method is appropriate for SRG in the low speed wind applications. To investigate the performance of the control system, a time series of turbulent dynamic wind speed is applied to the WECS as shown in Fig. 6. The performance of the proposed PBC method at different damping injection factors is investigated by obtaining the simulation results for the proposed PBC when CPL is increased from 260 W to 720 W in $t = 10s$, as an external disturbance and considering the limits in the applied CPL values to ensure both stable equilibria and internal stability of the controllers (17) and (21). The speed and dc-link voltage are shown in Figs. 7(a) and (b), respectively, when the additional damping terms are $R_{i1} = R_{i2} = 1/R_{i3} = R_{i4} = 1$ and $R_{i1} = R_{i2} = 5, 1/R_{i3} = R_{i4} = 10$, both of which are lower than their calculated maximum upper bounds. Fig. 7(b) shows the speed and the dc-link voltage with higher damping injection parameters; this allowed the wind profile to be tracked better than the PBC with low damping injection parameters shown in Fig. 7(a).

Clearly, increasing CPL to 720 W leads to a greater fluctuation in the speed and dc-link voltage when the damping injection terms are small. The increased nonlinearly of the system due to the increase in the CPL causes an error in the period of high applied CPL. A considerable robustness is achieved against the external load increase with increases in damping injection factors. The speed controller ensures the MPPT operation via the Tip Speed Ratio (TSR) technique [23]. It is seen that the oscillations in the speed response and phase current are lower when high damping injection terms are applied.

The frequency response is obtained after applying the proposed PBC, as shown in Fig. 8. The bode plot in Fig. 8 shows the phase margin increased from 34.8° to 90° in the increased bandwidth of 4340 Hz. The stability margin is improved, indicating the passivity of the converter for the target frequency spectrum. The delay phenomenon due to A/D sampling time, DSP calculation and PWM pattern generation are well investigated [24]. Based on the findings reported, the delay for this system can be modeled by e^{-sT_d}, where $T_d = 1.5T_{sw}$ and T_{sw} is the switching period. In our case

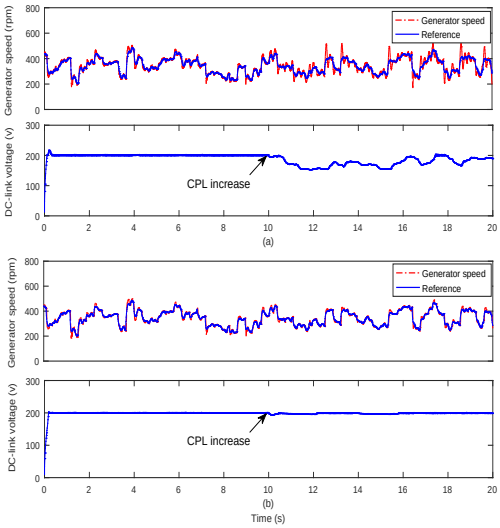

Fig. 7. Generator speed, and dc-link voltage under turbulent variable wind speed; (a) with low damping injection gains, (b) with high damping injection gains.

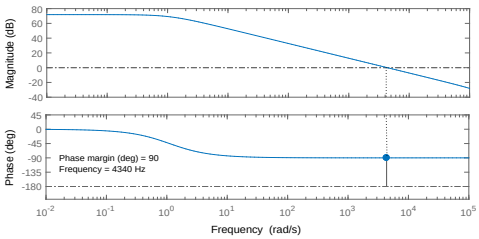

Fig. 8. Frequency response at 1200 W CPL with applying proposed PBC.

study where $f_{sw} = 10$ kHz, the total delay will reduce the phase margin from 90° down to 50° for a bandwidth of 4340 Hz, which is still above 45°, and is considered to be a safe margin.

2) Experimental Findings: To evaluate the performance of the proposed method, PBC with different damping injection terms is compared with a well-designed PI controller. Fig. 9(a) shows the measured values of steady-state dc-link voltage, one-phase current, and battery current in the charging mode when the power of the load is 260 W with applying PI controller. To illustrate the effectiveness of the proposed PBC method, Fig. 9(b) and (c) compare the results for the damping terms of $R_{i1} = 1/R_{i3} = R_{i4} = 1$ and $R_{i1} = 1/R_{i3} = R_{i4} = 10$, respectively. The capability of the proposed PBC in voltage control is more clearly realized when higher damping injection factors are applied, in which case a considerable robustness is achieved against the external CPL. Fig. 9(d) depicts this by showing the desired improvement during dc-link voltage and battery current fluctuations in the transition from a low to a high damping injection value. In all cases, the required CPL is lower than the generated power. Therefore, the the extra power is injected into the battery and causes the battery to charge, with the positive sign of the battery current.

To study the robustness when the load experiences a high

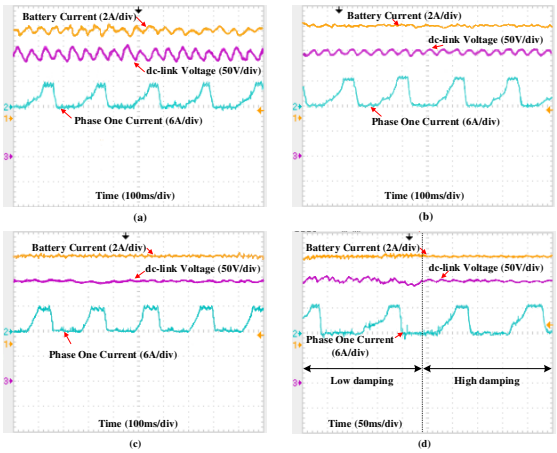

Fig. 9. DC-link voltage, charging current and phase current at 260 W CPL; (a) PI controller, (b) PBC with low damping, (c) PBC with high damping (d) with low to high damping factors transition.

step, Fig. 10(a) and (b) can be used to compare the dc-link voltage and battery current with low and high damped PBC with increasing CPL to 1200 W. As can be seen in Fig. 10(b), when optimum high damping injection terms are applied, the dc-link voltage is stable, and do not reset to the battery voltage value which is contrary to the condition shown in Fig. 10(a). It can be seen that in the case of using optimum damped PBC, the bidirectional converter changes from charging to discharging mode whenever dc-link voltage is decreased to the battery voltage in the high CPL.

The experimental results obtained for the variable turbulent wind speed control are presented in Fig. 12(a) and (b). The dc-link voltage and the generator speed related to the pre-defined time-varying wind speed profile are illustrated for both low and high CPL levels when the CPL increases in $t = 10s$. Figure 12(a) demonstrates the SRG-based WECS performance with low damping factors, while Fig. 12(b) shows the results when the optimum higher damping injection gains are applied. According to Fig. 12(b), CPL variations will affect neither the MPPT nor the dc-link voltage control performance when an optimum high damping injection is employed. The dc-link voltage is controlled while the wind speed exhibits significant variations. However, higher voltage ripples are observed at the high CPL step.

The results of using the PBC indicate a good tracking, with no overshoot or undershoot in the generator speed by using the proposed PBC. Based on these results obtained, the PBC is well capable of controlling the system with acceptably low ripples in speed and voltage and with a fast dynamic while also converging to the command with a near zero steady-state error.

VI. Conclusions

This study conducted a system-level modeling of the SRG-based DC microgrid considering the interaction of SRG and constant power load dynamic characteristics. A complete Euler-Lagrange mathematic model of the SRG-based DC microgrid was provided as the interconnection of the two electrical and mechanical passive linked subsystems. Considering the

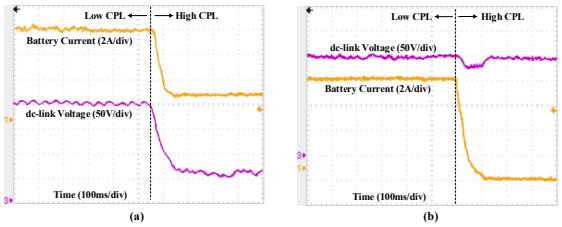

Fig. 10. DC-link voltage and battery current; (a) Unstable response to CPL high step increase with low damping factors, (b) Stable response to CPL high step increase with high damping factors.

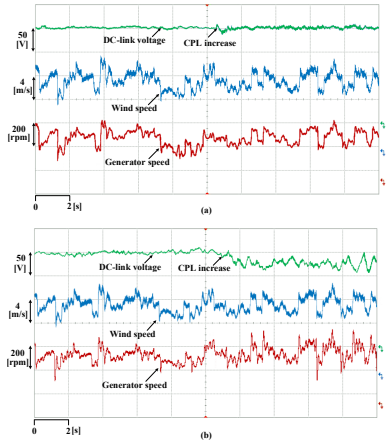

Fig. 11. Generator speed and dc-link voltage under variable driven wind speed; (a) with low-damped PBC, (b) with optimum high-damped PBC.

two subsystem passivity properties, an MPPT was developed based on speed control and dc-link voltage regulation using a proposed EL-based PBC technique. As the uncertainty associated with the physical structure of the SRG was taken into account by means of an adaptation mechanism, the MPPT was able to overcome its inherent complicated dynamic characteristics and input voltage variations. The active damping injection in the system through the PBC resulted in the diminishing of undamped oscillations, enhanced the stability of the system, and decreased the destabilizing effect of CPL. The controller is shown to be effective to compensate uncertainties caused by the back-EMF and position-dependent phase inductance variations. The obtained simulation and experimental results demonstrate the properties of the proposed PBC which shows improved dynamic of rotor speed and lower dc-link voltage ripples.

Appendix A
Calculation of i_b^*

The desired reference command for battery current can be determined from the steady state solution of 9 as

$$i_{\mathrm{b}}^{*}=\frac{\frac{P_{\mathrm{cpl}}}{V_{\mathrm{c}}^{*}}-\sum_{\mathrm{j}=1}^{4}\left(1-d_{\mathrm{j}}\right)i_{\mathrm{j}}^{*}}{\left(1-d_{\mathrm{b}}\right)} \tag{31}$$

where $(1-d_b)$ is obtained from the steady state solution of 8 as

$$1-d_{\mathrm{b}}=\frac{V_{\mathrm{b}}-i_{\mathrm{b}}^{*}R_{\mathrm{b}}}{V_{\mathrm{c}}^{*}} \tag{32}$$

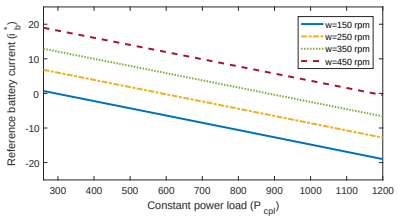

Fig. 12. Variations of i_b^* under changes in the wind speed and CPL.

Substituting 32 in 31, we deduce the following quadratic equation

$$-R_{\mathrm{b}}i_{\mathrm{b}}^{*2}+V_{\mathrm{b}}i_{\mathrm{b}}^{*}+\sum_{\mathrm{j}=1}^{4}\left(1-d_{\mathrm{j}}\right)i_{\mathrm{j}}^{*}V_{\mathrm{c}}^{*}-P_{\mathrm{cpl}}=0 \tag{33}$$

Then, the desired reference command for battery current is obtained by solving 33 for i_b^* as

$$i_{\mathrm{b}}^{*}=\frac{V_{\mathrm{b}}}{2R_{\mathrm{b}}}-\sqrt{\left(\frac{V_{\mathrm{b}}}{2R_{\mathrm{b}}}\right)^{2}+\frac{\sum_{\mathrm{j}=1}^{4}\left(k_{\mathrm{j}}\left(\theta\right)\omega_{\mathrm{m}}^{*}-r\right)i_{\mathrm{j}}^{*2}V_{\mathrm{c}}^{*}-P_{\mathrm{cpl}}}{R_{\mathrm{b}}}} \tag{34}$$

where $(1-d_j)$ is substituted from 7 under steady state condition. The average value of back-emf coefficient, which is used in 34 is -0.15 . Figure 12 shows the graphs of boundaries for i_b^* based on 34 considering the variation of the wind speed and CPL. The graphs show the battery current reference is changed as a function of the capture wind power and the consumed power by CPL. Based on these graphs, i_b^* is selected as -1 A in discharging mode and 7 A in charging mode.

References

[1] Z. Alnasir and M. Kazerani, "An analytical literature review of stand-alone wind energy conversion systems from generator viewpoint," *Renewable and Sustainable Energy Reviews*, vol. 28, pp. 597 – 615, 2013.

[2] N. A. Orlando, M. Liserre, R. A. Mastromauro, and A. Dell'Aquila, "A survey of control issues in pmsg-based small wind-turbine systems," *IEEE Transactions on Industrial Informatics*, vol. 9, no. 3, pp. 1211–1221, Aug 2013.

[3] Y. C. Chang and C. M. Liaw, "Establishment of a switched-reluctance generator-based common dc microgrid system," *IEEE Transactions on Power Electronics*, vol. 26, no. 9, pp. 2512–2527, Sept 2011.

[4] V. Valdivia, R. Todd, F. J. Bryan, A. Barrado, A. Lzaro, and A. J. Forsyth, "Behavioral modeling of a switched reluctance generator for aircraft power systems," *IEEE Transactions on Industrial Electronics*, vol. 61, no. 6, pp. 2690–2699, June 2014.

[5] M. Cespedes, L. Xing, and J. Sun, "Constant-power load system stabilization by passive damping," *IEEE Transactions on Power Electronics*, vol. 26, no. 7, pp. 1832–1836, July 2011.

[6] A. M. Rahimi and A. Emadi, "Active damping in dc/dc power electronic converters: A novel method to overcome the problems of constant power loads," *IEEE Transactions on Industrial Electronics*, vol. 56, no. 5, pp. 1428–1439, May 2009.

[7] X. Chang, Y. Li, X. Li, and X. Chen, "An active damping method based on a supercapacitor energy storage system to overcome the destabilizing effect of instantaneous constant power loads in dc microgrids," *IEEE Transactions on Energy Conversion*, vol. 32, no. 1, pp. 36–47, March 2017.

[8] S. C. Smithson and S. S. Williamson, "A novel control strategy for dc-dc converters driving constant power loads," in *2013 IEEE International Conference on Industrial Technology (ICIT)*, Feb 2013, pp. 1796–1801.

[9] H. J. Kim, S. W. Kang, G. S. Seo, P. Jang, and B. H. Cho, "Large signal stability analysis of dc power system with shunt active damper," *IEEE Transactions on Industrial Electronics*, vol. PP, no. 99, pp. 1–1, 2016.

[10] T. A. dos Santos Barros, P. Neto, P. Nascimento, A. Moreira, and E. R. Filho, "An approach for switched reluctance generator in wind generation system with wide range of operation speed," *IEEE Transactions on Power Electronics*, vol. PP, no. 99, pp. 1–1, 2017.

[11] J. Wang, X. Mu, and Q. K. Li, "Study of passivity-based decoupling control of t-npc pv grid-connected inverter," *IEEE Transactions on Industrial Electronics*, vol. 64, no. 9, pp. 7542–7551, Sept 2017.

[12] J. Zeng, Z. Zhang, and W. Qiao, "An interconnection and damping assignment passivity-based controller for a dc-dc boost converter with a constant power load," *IEEE Transactions on Industry Applications*, vol. 50, no. 4, pp. 2314–2322, July 2014.

[13] R. Cisneros, F. Mancilla-David, and R. Ortega, "Passivity-based control of a grid-connected small-scale windmill with limited control authority," *IEEE Journal of Emerging and Selected Topics in Power Electronics*, vol. 1, no. 4, pp. 247–259, Dec 2013.

[14] M. D. Benedetto, A. Lidozzi, L. Solero, F. Crescimbini, and P. J. Grbovic, "Small-signal model of the five-level unidirectional t-rectifier," *IEEE Transactions on Power Electronics*, vol. 32, no. 7, pp. 5741–5751, July 2017.

[15] R. Ortega, A. Loria, P. J. Nicklasson, and H. Sira-Ramirez, *Passivity-based Control of Euler-Lagrange Systems. Mechanical, Electrical and Electromechanical Applications*. Springer-Verlag, 1998.

[16] S. Bacha, I. Munteanu, and A. I. Bratcu, *Power Electronic Converters Modeling and Control: with Case Studies*. Springer-Verlag, 2014.

[17] A. Dell'Aquila, M. Liserre, V. G. Monopoli, and P. Rotondo, "An energy-based control for an n-h-bridges multilevel active rectifier," *IEEE Transactions on Industrial Electronics*, vol. 52, no. 3, pp. 670–678, June 2005.

[18] D. del Puerto-Flores, J. M. A. Scherpen, M. Liserre, M. M. J. de Vries, M. J. Kransse, and V. G. Monopoli, "Passivity-based control by series/parallel damping of single-phase pwm voltage source converter," *IEEE Transactions on Control Systems Technology*, vol. 22, no. 4, pp. 1310–1322, July 2014.

[19] B. Fahimi, A. Emadi, and R. B. Sepe, "A switched reluctance machine-based starter/alternator for more electric cars," *IEEE Transactions on Energy Conversion*, vol. 19, no. 1, pp. 116–124, March 2004.

[20] C. Cecati, A. Dell'Aquila, M. Liserre, and V. G. Monopoli, "A passivity-based multilevel active rectifier with adaptive compensation for traction applications," *IEEE Transactions on Industry Applications*, vol. 39, no. 5, pp. 1404–1413, Sept 2003.

[21] E. Roshandel, M. M. Namazi, A. Rashidi, S. M. Saghaian-Nejad, and J. W. Ahn, "Ssc strategy for srg to achieve maximum power with minimum current ripple in battery charging," *IET Electric Power Applications*, vol. 11, no. 7, pp. 1205–1213, 2017.

[22] A. Khaligh, A. M. Rahimi, and A. Emadi, "Modified pulse-adjustment technique to control dc/dc converters driving variable constant-power loads," *IEEE Transactions on Industrial Electronics*, vol. 55, no. 3, pp. 1133–1146, March 2008.

[23] M. C. D. Piazza and M. Pucci, "Induction-machines-based wind generators with neural maximum power point tracking and minimum losses techniques," *IEEE Transactions on Industrial Electronics*, vol. 63, no. 2, pp. 944–955, Feb 2016.

[24] L. Harnefors, R. Finger, X. Wang, H. Bai, and F. Blaabjerg, "Vsc input-admittance modeling and analysis above the nyquist frequency for passivity-based stability assessment," *IEEE Transactions on Industrial Electronics*, vol. 64, no. 8, pp. 6362–6370, Aug 2017.

Mohammad Masoud Namazi (S'09) was born in Isfahan, Iran, in 1986. He received the B.Sc. in electrical engineering from Shahed University, Tehran, Iran, in 2009 and the M.Sc. in electrical engineering from Isfahan University of Technology, Isfahan, Iran, in 2011, where he is currently working toward the Ph.D. degree in the Department of Electrical and Computer Engineering. He was a visiting researcher in smart mechatronics lab in Kyungsung University, Busan, Korea from September 2014 to May 2015. His fields of research are electric drives, nonlinear control, microgrids and renewable energy systems.

Sayed Morteza Saghaian Nejad received his B.S., M.S. and Ph.D. in Electrical Engineering from the University of Kentucky, USA in 1977, 1979 and 1989, respectively. Since 1979, he has been a faculty member of Isfahan University of Technology, where he is currently a Professor in electrical and computer engineering department. He is the author or coauthor of various journal and conference papers. His research interests include analysis and control of electrical machines, control of electrical drives, power electronics, and switched reluctance machines.

Ahmadreza Tabesh (S01, M06) received the Ph.D. degree in electrical engineering (Energy Systems) from the University of Toronto, Toronto, ON, Canada, in 2005. He was postdoctoral fel- low and research associate with the Center for Applied Power Electronics, University of Toronto (2005-06) and the Microengineering Laboratory for MEMS, Department of Mechanical Engineer- ing, University of Sherbrooke, Sherbrooke, QC, Canada (2006-09). Currently, he is an Associate Professor in the Department of Electrical and Computer Engineering, Isfahan University of Technology, Isfahan, Iran. His research interests include grid integration of renewable energy resources, dc microgrids, energy harvesters for powering of Internet- of-Things (IoT) devices.

Amir Rashidi received the M.S. and Ph.D. degrees from Isfahan University of Technology, Isfahan, Iran, in 2009, and 2016. He was a visiting researcher in smart mechatronics lab in Kyungsung University, Busan, Korea from September 2014 to July 2015. He was chosen as the best Ph.D. student in Isfahan University of Technology in 2014. He was also the recipient of the Student Awards Yearbook in 2015 . His research interests include electric motor drives, power electronics and microprocessor-based control systems.

Marco Liserre (S'00-M'02-SM'07-F13) received the MSc and PhD degree in Electrical Engineering from the Bari Polytechnic, respectively in 1998 and 2002. He has been Associate Professor at Bari Polytechnic and Professor at Aalborg University (Denmark). He is currently Full Professor and he holds the Chair of Power Electronics at Christian-Albrechts-University of Kiel (Germany). He has published over 300 technical papers (more than 100 of them in international peer-reviewed journals) and a book. These works have received more than 20000 citations. Marco Liserre is listed in ISI Thomson report The worlds most influential scientific minds. He is member of IAS, PELS, PES and IES. He has been serving all these societies in different capacities and he has received several IEEE awards.